

HF-DGF: Hybrid Feedback Guided Directed Grey-box Fuzzing

Guangfa Lyu*, Zhenzhong Cao[†], Xiaofei Ren*, Fengyu Wang*^{‡§}

**School of Software, Shandong University, Jinan, China*

[‡]*Quan Cheng Laboratory, Jinan, China*

[†]*School of Cyber Science and Engineering, Qufu Normal University, Qufu, China*

Abstract—Directed Grey-box Fuzzing (DGF) has emerged as a widely adopted technique for crash reproduction and patch testing, leveraging its capability to precisely navigate toward target locations and exploit vulnerabilities. However, current DGF tools are constrained by insufficient runtime feedback, limiting their efficiency in reaching targets and exploring state spaces.

This study presents HF-DGF, a novel directed grey-box fuzzing framework. Its seed scheduling is guided by a hybrid feedback mechanism integrating control-flow distance, value-flow influence score, and slice coverage. To enable precise control-flow distance feedback, we propose a backward-stepping algorithm to calculate basic block-level seed distances on a virtual inter-procedural control-flow graph (ICFG). For effective state space exploration, we introduce value-flow influence and a corresponding metric, the value-flow influence score. Additionally, to mitigate runtime overhead from hybrid feedback, we adopt a novel selective instrumentation strategy.

Evaluations on 41 real-world vulnerabilities show HF-DGF outperforms existing tools: it achieves crash reproduction $5.05\times$ faster than AFL, $5.79\times$ faster than AFLGo, $73.75\times$ faster than WindRanger, $2.56\times$ faster than DAFL, and $8.45\times$ faster than Beacon on average. Notably, when all fuzzers triggered crashes, HF-DGF exhibited the lowest code coverage, demonstrating superior directionality and efficiency. It also surpasses AFLGo, WindRanger, DAFL, and Beacon in static analysis efficiency.

Index Terms—Directed Grey-box Fuzzing, Static Analysis, Hybrid Feedback, Selective Instrumentation

I. INTRODUCTION

Grey-box fuzzing [1]–[3] has been widely employed in uncovering vulnerabilities in real-world software, including parsers [4], [5], web browsers [6], [7], OS kernels [8]–[11], and network protocols [12]–[14].

For effective testing of pre-determined target locations in large-scale programs, Directed Grey-box Fuzzing (DGF) has been proposed. In contrast to Coverage-guided Grey-box Fuzzing (CGF), which allocates uniform attention across various code sections to maximize overall code coverage, DGF prioritizes efficient navigation towards specified target locations for in-depth testing. This feature has facilitated its extensive adoption in diverse scenarios: identifying regression bugs by focusing on recently modified code [15], testing vulnerability patches by targeting patched code sites [16],

[17], reproducing crashes by concentrating on crashing sites [18], [19], verifying static analysis reports by designating suspicious locations as targets, and tracking information flow by specifying source-sink pairs [20].

The performance of a directed grey-box fuzzer hinges on three critical dimensions: (1) *target convergence efficiency*—the ability to rapidly reach target locations; (2) *state space exploration effectiveness*—the capability to thoroughly explore the target state space; (3) *runtime overhead optimization*—the capacity to minimize unnecessary instrumentation costs.

A. Limitations of Existing Approaches

1) *Imprecise Path Navigation*: Most existing DGFs rely on coarse-grained seed distance estimations. For example, AFLGo [21] determines basic block distances primarily based on function-level distances from the call graph, overlooking intra-function logical discrepancies. Moreover, indirect calls—prevalent in languages like C/C++—are inadequately modeled in call graphs, leading to significant distance calculation errors. These limitations severely degrade navigation precision.

2) *Inadequate State Space Exploration*: Current DGFs often prioritize proximity to targets while neglecting state space exploration. However, vulnerabilities like buffer overflows impose strict value constraints, requiring not only target reachability but also extensive state exploration. Existing methods lack mechanisms to balance *proximity-driven navigation* and *state-space exploration*, hindering vulnerability triggering efficiency.

3) *High Runtime Overhead*: To obtain runtime feedback, conventional DGFs employ extensive instrumentation: full instrumentation of all basic blocks for coverage feedback and distance-based instrumentation of only reachable basic blocks. This heavy instrumentation introduces substantial runtime overhead, necessitating strategies to minimize unnecessary instrumentation while preserving feedback effectiveness.

B. Our Approach: HF-DGF

This paper presents HF-DGF, an advanced directed grey-box fuzzing framework addressing the above limitations. HF-DGF innovatively integrates three orthogonal feedback mechanisms—control-flow distance, value-flow influence score, and slice coverage—into a hybrid feedback-driven seed scheduling system, complemented by a selective instrumentation strategy to mitigate overhead. By leveraging fine-grained

This work was supported by the Key Project of Quan Cheng Laboratory (QCLZD202304), and the Project of Provincial Laboratory of Shandong (SYS202201).

[§]Corresponding author: Fengyu Wang, Email: wangfengyu@sdu.edu.cn

control-flow distance for efficient target navigation and combining value-flow influence scores (quantifying dependency strength) with slice coverage (quantifying dependency scope) for systematic state space exploration, HF-DGF enables rapid and comprehensive target traversal—a capability overlooked by traditional single-feedback fuzzers. This synergistic integration establishes a “reach-then-explore” paradigm that significantly enhances both the efficiency of target convergence and the effectiveness of vulnerability discovery.

C. Experimental Validation

We evaluated HF-DGF using DAFL’s benchmark dataset [22], which contains 41 vulnerabilities from the AFLGo benchmark and 9 real-world programs. Key results:

- **Rapid Target Convergence:** HF-DGF cuts the time to reach target locations and trigger crashes across all test cases, achieving an average speedup of $2.56\text{--}73.75\times$ over state-of-the-art baselines.
- **Efficient Vulnerability Triggering:** By systematically exploring target state spaces, HF-DGF triggers more vulnerabilities in 24 hours: $1.16\times$ more than AFL, $1.12\times$ more than AFLGo, $1.45\times$ more than WindRanger, $1.14\times$ more than DAFL, and $1.56\times$ more than Beacon.
- **Overhead Optimization:** Using selective instrumentation, HF-DGF reduces code coverage by 80.9% vs. traditional full-instrumentation fuzzers (AFL/AFLGo/WindRanger), reaching only 54.8% of DAFL’s coverage while maintaining high vulnerability discovery rates.
- **Component Synergy Validation:** Ablation studies show control-flow distance, value-flow influence scores, and slice coverage drive performance gains. Integrating these techniques reproduces vulnerabilities $6.98\times$ faster than AFLGo.

D. Contributions

The main contributions of this paper are summarized as follows:

- **Novel Framework Design:** We propose HF-DGF, addressing ambiguous navigation, insufficient exploration, and high overhead via integrating three orthogonal feedback mechanisms (control-flow distance, value-flow influence score, slice coverage) into a hybrid feedback-driven seed scheduling system, enabling a “reach-then-explore” paradigm.
- **Precise Distance Calculation:** A backward-stepping approach is devised to compute fine-grained basic-block-level seed distances, resolving navigation ambiguity in traditional fuzzers.
- **Enhanced State Exploration:** Value-flow influence score (dependency strength) and slice coverage (dependency scope) collaborate to systematically traverse target state spaces, amplifying exploration of unvisited target state spaces.
- **Overhead Optimization:** A selective instrumentation strategy is implemented to mitigate runtime overhead inherent to hybrid feedback. This balances feedback richness and performance, ensuring efficiency without compromising exploration thoroughness.

- **Comprehensive Validation:** We develop a HF-DGF prototype and conduct extensive experiments. HF-DGF outperforms state-of-the-art fuzzers in both efficiency and effectiveness.

II. MOTIVATION

In this section, we illustrate the motivation behind our research by analyzing the key challenges confronting current directed grey-box fuzzers.

A. Inaccurate control-flow distance calculation

Existing DGF tools primarily rely on control-flow distance to guide fuzzing, yet inaccuracies in this metric can induce path selection bias.

Given a target basic block T_b within target function T_f , AFLGo first calculates the function-level distance $d_f(f, T_f)$ as the shortest distance from function f to T_f within the call graph. Then, AFLGo computes the basic block-level distance between basic block s and target basic block T_b using Equation 1:

$$D(s, T_b) = \left[\sum_{m \in G(s)} (d_b(s, m) + c \cdot \min_{f \in F(m)} d_f(f, T_f))^{-1} \right]^{-1} \quad (1)$$

where $G(s)$ is the set of basic blocks within the control-flow graph of s that call target-reachable functions. $d_b(s, m)$ is the distance from basic block s to m (where m invokes a target-reachable function), $F(m)$ represents the target-reachable functions called by basic block m , $d_f(f, T_f)$ denotes the function-level distance, and the constant c is typically set to 10 in practice.

The computation of basic block-level distance relies on function-level distance derived from the call graph, which ignores intra-function logic differences. This oversight compromises the accuracy of basic block-level distance metrics. Moreover, when the target location is deep within program logic, errors accumulate through each traversed function, exacerbating the discrepancy between calculated and actual distances.

Other state-of-the-art approaches inherently share similar limitations. For example, WindRanger [23] calculates distances between deviation basic blocks under the assumption that all functions are equidistant, overlooking internal structural differences. Meanwhile, although Hawkeye enhances proximity measurement by incorporating the number and distribution of call sites derived from static analysis, it still lacks precision in basic block distance calculation due to its ignorance of call site depths within intermediate functions. This gap underscores the necessity of a novel approach to accurately compute control-flow distances.

B. Insufficient exploration of target state space

It is widely acknowledged that certain vulnerabilities are only triggered under specific data conditions. For instance, a typical buffer overflow vulnerability is more likely to occur when the input seed approaches the boundary of the vulnerable buffer [24]. Existing DGF tools like AFLGo primarily focus on control-flow guidance to aid in reaching target locations,

yet they often overlook exploration of the target state space—a subset of the program state space inherently linked to target locations. This oversight impedes effective fuzzing from satisfying the specific data conditions required to trigger vulnerabilities.

Data-flow influence feedback can serve as a guiding mechanism for exploring the target state space. However, the underutilization of data-flow information significantly impedes its effectiveness in guiding fuzzing, leading to suboptimal exploration of the target state space. SelectFuzz [25] identifies code sections for selective instrumentation by leveraging data dependencies, but fails to fully capitalize on data-flow information for seed scheduling. WindRanger [23] utilizes taint analysis to collect data-flow information impacting branch constraints, yet its byte-by-byte mutation and feedback collection introduce substantial runtime overhead. These limitations underscore the necessity of introducing value-flow influence as an effective means to explore the target state spaces.

III. OVERVIEW OF HF-DGF

In this section, we present a brief overview of HF-DGF, with particular emphasis on clarifying its core mechanism: path selection.

A. Structure and Workflow

The overall architecture of HF-DGF is depicted in Fig. 1, which consists of three core components: static analyzer, selective instrumenter, and fuzzer. These components collaborate to enable hybrid feedback-driven fuzzing, and their workflow is structured as follows.

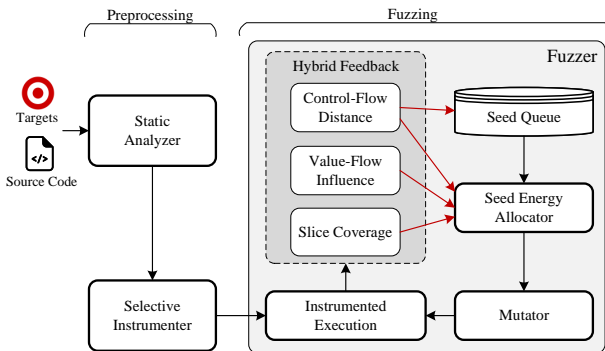


Fig. 1: Overview of HF-DGF.

First, the static analyzer performs in-depth analysis on the target program’s source code. It constructs function call graphs, control-flow graphs (CFGs), and value-flow graphs (VFG) to model execution logic and data dependencies. For target-reachable basic blocks, it calculates two key metrics at the basic-block level: control-flow distance (measuring structural proximity to the target in the CFG) and value-flow influence score (quantifying data-flow impact on the target via the VFG). Additionally, it slices these target-reachable basic blocks and identifies boundary basic blocks (those with no sliced successors), which together define the scope for

selective instrumentation to ensure only critical regions are instrumented.

Next, the selective instrumenter injects code into the target program based on the static analysis results. Specifically, it instruments sliced basic blocks to obtain slice coverage feedback, boundary basic blocks to capture distance feedback, and blocks with value-flow influence scores to generate value-flow influence feedback. This targeted instrumentation minimizes overhead while ensuring feedback directly reflects the target context.

Finally, the fuzzer executes the instrumented program and leverages runtime feedback for seed scheduling and energy allocation. Seed prioritization is determined by distance to the target (closer seeds get higher priority), and seed energy (number of mutations) is computed by integrating slice coverage, control-flow distance, and value-flow influence. Seeds with higher slice coverage, shorter distances, and stronger value-flow influence receive more mutations, directing fuzzing efforts toward high-potential paths and accelerating vulnerability discovery.

In summary, the workflow of HF-DGF commences with static analysis to map the program structure and delineate the instrumentation scope, proceeds to selective instrumentation for the collection of targeted feedback, and culminates in feedback-driven fuzzing that prioritizes seeds and strategically allocates mutation energy.

B. Path Selection

To elucidate the underlying rationale of the HF-DGF system, we exemplify how seed prioritization and energy allocation influence path selection.

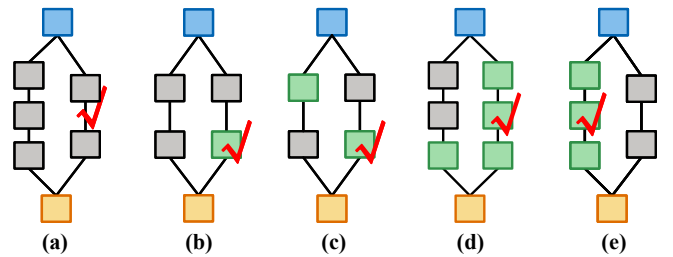


Fig. 2: Path Selection in HF-DGF.

As depicted by the CFGs in Fig. 2, blue blocks signify entry points, yellow blocks indicate crash-trigger points, and green blocks represent basic blocks that directly or indirectly impact the target value. In Fig. 2a, two paths exist, differing only in distance with no alterations to the target value. Consequently, HF-DGF gives precedence to the shorter path. In Fig. 2b, despite both paths reaching the target at an equal distance, the right-hand path contains a basic block that modifies the target value. Thus, HF-DGF favors the right-hand path. Fig. 2c shows two paths, both modifying the target value. However, the basic block influencing the target value on the right-hand path is nearer, resulting in a more direct influence. Hence, HF-DGF exhibits a preference for the right-hand path. In Fig. 2d, both paths include basic blocks modifying the target value. Yet, the right-hand path has more such blocks, leading to

a more extensive value-flow influence and a more thorough exploration of the target state space. Therefore, HF-DGF inclines towards the right-hand path. For the scenarios in Fig. 2e, where paths vary in both distance to the target location and target-value modifications. Initially, HF-DGF explores the shorter right-hand path. But since it doesn't involve value modifications, HF-DGF allocates less energy to it. When it reaches the left-hand path, which has a stronger value-flow influence, HF-DGF assigns more energy to the seed, enabling comprehensive exploration of the target state space.

IV. DESIGN OF HF-DGF

The fuzzing design of HF-DGF hinges on integrating three key feedbacks: control-flow distance, value-flow influence score, and slice coverage. This section first details the calculations for control-flow distance and value-flow influence score. It then presents the selective instrumentation strategy to acquire these three feedbacks. Finally, it explains how the multi-dimensional feedback drives seed prioritization and energy allocation in fuzzing.

A. Control-flow distance

In directed grey-box fuzzing, seed distance feedback is critical for steering the exploration towards target locations. While our approach, similar to AFLGo, computes distances at the basic block level via static analysis and determines seed distances during fuzzing, we innovate by constructing a virtual ICFG and designing a backward-stepping distance calculation algorithm to compute control-flow distances of basic blocks rapidly and precisely. The following subsections detail our methodology in HF-DGF.

Basic-Block Distance: Traditional function-level distance calculation based on call graphs is coarse-grained. By treating function calls as basic block transitions and unwrapping functions to the basic-block level, we derive fine-grained basic-block distances, defined as the shortest path length from a basic block to the target within an ICFG.

However, constructing a comprehensive path-sensitive ICFG is impractical due to its scale, so we adopt a backward-stepping strategy for basic-block distance calculation in a virtual ICFG. This strategy decomposes the calculation into four manageable steps for accuracy, which we illustrate using Fig. 3.

First, we identify functions reachable to the target location via function call sequences (e.g., functions *A*, *B*, *C* marked in Fig. 3a) using breadth-first traversal on the function call graph, expanding the scope with Andersen-style pointer analysis [26] to handle indirect calls. During traversal, we record call-site basic blocks (**yellow** in Fig. 3) invoking these reachable functions.

Next, we compute the depth of each call-site basic block as the shortest path length from the entry basic block (**blue** in Fig. 3) within the control-flow graph. For example, in Fig. 3b, the depths of *A3*, *B3*, and *C4* are 1, 2, and 2, respectively.

In the third step, we calculate distances from both call-site and entry basic blocks to the target. For a call-site basic block, its distance is the called function's entry block distance plus

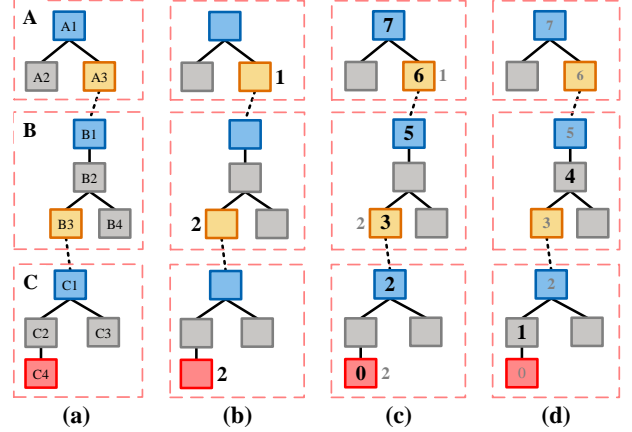


Fig. 3: Basic-block Distance Calculation in HF-DGF.

1 (choosing the minimum if multiple functions are invoked). For an entry basic block, its distance is the sum of the depth and distance of the call-site basic block within the same function (taking the minimum sum if multiple call sites exist). Given the interdependency of these calculations, we follow Algorithm 1, computing distances for blocks *C1*, *B3*, *B1*, *A3*, *A1* sequentially, as shown in Fig. 3c.

Finally, for the control-flow graph of each function reachable to the target location (i.e., functions capable of reaching the target via call graph traversal), we perform a reverse breadth-first traversal from its call-site basic block, tracking the number of traversed layers. The distance of each traversed block is the call-site block's pre-determined distance plus the layer count. For instance, in Fig. 3d, the distances of *C2* and *B2* are 1 and 4, respectively.

More formally, the basic-block distance is defined by Equation 2.

$$Distance(bb, t) = \begin{cases} 0 & bb = t \\ \min_{f \in CF(bb)} Distance(Entry(f), t) + 1 & bb \in CS(bb) \\ \min_{cs \in CS(bb)} [Depth(bb) + Distance(cs, t)] & bb \in Entries \\ \min_{cs \in CS(bb)} [dbb(bb, cs) + Distance(cs, t)] & bb \in Reach(t) \end{cases} \quad (2)$$

where, $dbb(bb, cs)$ is the shortest length from basic block bb to cs within the control-flow graph; *call-sites* represents all call-site basic blocks; *Entries* denotes the entry basic blocks of all sliced functions; *Reach*(t) contains the basic blocks from which the target basic block t is reachable along the control-flow; *CF*(bb) signifies the functions called by the `call` instructions within the basic block bb ; and *CS*(bb) refers to all call-site basic blocks within the function in which bb resides.

When multiple target locations exist, we compute the distance from a basic block to each target independently and then use the *harmonic mean* to derive the block's final distance, as defined in Equation 3. This approach ensures the distance metric accounts for proximity to all targets.

Algorithm 1 Backward-Stepping Distance Calculation.

Require: $target_bb, depth$
Ensure: $distance$

```

1:  $target\_function \leftarrow GETFUNCTION(target\_bb)$ 
2:  $distance[target\_bb] \leftarrow 0$ 
3:  $distance[target\_function] \leftarrow 0$ 
4:  $function\_queue \leftarrow \{target\_function\}$ 
5: while  $function\_queue$  is not empty do
6:    $callee \leftarrow function\_queue.dequeue()$ 
7:   for all  $callsite$  in  $GETCALLSITES(callee)$  do
8:      $caller \leftarrow GETFUNCTION(callsite)$ 
9:      $dist \leftarrow distance[callee] + 1$ 
10:    if  $distance[callsite] > dist$  then
11:       $distance[callsite] \leftarrow dist$ 
12:    end if
13:     $dist \leftarrow distance[callsite] + depth[callsite]$ 
14:    if  $distance[caller] > dist$  then
15:       $distance[caller] \leftarrow dist$ 
16:       $function\_queue.enqueue(caller)$ 
17:    end if
18:  end for
19: end while

```

$$Distance(bb, T) = \left[\sum_{t \in T} Distance(bb, t)^{-1} \right]^{-1} \quad (3)$$

Seed Distance: Seed distance measures the proximity of a seed’s execution path to the target location. Unlike AFLGo [27] and HawkEye [28], which compute this metric using all basic blocks, HF-DGF innovatively averages the precomputed control-flow distances of boundary basic blocks. For a target set T , the distance of seed s is defined as:

$$Distance(s, T) = \frac{\sum_{bb \in \Phi(s)} Distance(bb, T)}{|\Phi(s)|} \quad (4)$$

where $Distance(bb, T)$ represents the precomputed control-flow distance from basic block bb to T , and $\Phi(s)$ denotes the set of boundary blocks in s ’s execution trace.

This seed distance calculation method offers two key advantages. First, by focusing on boundary basic blocks, it minimizes instrumentation and feedback collection overhead by eliminating redundant monitoring of non-critical code. Second, by using the boundaries of reachable code as the metric, it enables precise seed distance measurement—outperforming traditional all-block averaging methods in both efficiency and accuracy.

B. Value-flow influence

Data-sensitive vulnerabilities (e.g., buffer overflows) depend on specific target data states, not just target location reachability. To tackle this, HF-DGF introduces value-flow influence and a novel fitness metric: the value-flow influence score. Unlike DAFL, which uses data-flow analysis to slice basic blocks and compute control-flow distances, HF-DGF employs the value-flow influence score to quantify a seed’s

ability to explore target state spaces. The score aggregates influence contributions from all impactful basic blocks along the execution path, inherently prioritizing multi-stage target data manipulation paths. This accumulative scoring strategy enables systematic exploration of complex state spaces, improving the detection of data-sensitive vulnerabilities by guiding fuzzing efforts toward critical data dependencies.

Value-flow Influence: In program analysis, value flow [29] refers to the transfer of variable values during program execution through assignments and *def-use* chains. Previous studies [30], [31] have demonstrated that analyzing program value flow can effectively detect potential vulnerabilities. This underlines the significance of integrating value-flow analysis when modeling data modification and transfer in programs.

Inspired by these findings, we use value flow to guide fuzzing for efficient exploration of the program’s target state space. Basic blocks directly or indirectly modifying target data have a value-flow influence. We assign distinct weights, called value-flow influence scores, to these basic blocks. Blocks nearer the target location get higher scores. HF-DGF tracks and accumulates the value-flow influence scores of covered basic blocks for one seed, which becomes the seed’s value-flow influence score. A higher score implies the seed is more beneficial for exploring the target state space.

Value-flow Influence Score of Seed: We compute a seed’s value-flow influence score in two phases. First, in static analysis, we obtain basic-block-level value-flow influence scores. Then, during fuzzing, we determine the final seed-level score.

The value-flow influence score is derived from the value-flow graph. To identify complex pointer references and structure sub-fields, we enhance the value-flow graph using field-sensitive Anderson-style pointer analysis. In this graph, instructions modifying target data are nodes, and their influence on target data depends on their proximity to it. Thus, we initially calculate the distance from each instruction to the target data using the value-flow graph. For a given target data t , we define the value-flow distance of instruction i as:

$$VFD(i, t) = \begin{cases} \text{undefined} & i \notin Reach(t) \\ 0 & i = t \\ \min_{si \in Succ(i, t)} VFD(si, t) + 1 & i \in Reach(t) \end{cases} \quad (5)$$

For scenarios with multiple targets, a single instruction can impact multiple data points. To measure an instruction’s influence on a multi-target set T , we define the instruction-level value-flow influence ($VFI(i, T)$) as:

$$VFI(i, T) = \frac{\sum_{v \in V(T)} [\max VFD - VFD(i, v)]}{|V(T)|} \quad (6)$$

where $V(T)$ consists of all targets within the multi-target set T , and $VFD(i, v)$ denotes the value-flow distance from instruction i to a specific target v . Essentially, instructions closer to the targets are assigned a higher value-flow influence.

Next, we calculate the basic-block-level value-flow influence as the *minimum* of all instruction-level value-flow influences within the block. For a basic block bb with a set of instructions ins , we define its value-flow influence VFB as:

$$VFB(bb, T) = \min_{i \in ins} VFI(i, T) \quad (7)$$

The seed-level value-flow influence score VFS is computed during the fuzzing process. Let $\Phi(s)$ represent the execution trace of seed s , encompassing executed basic blocks with value-flow influence. We define the seed’s value-flow influence score VFS as follows:

$$VFS(s, T) = \sum_{bb \in \Phi(s)} VFB(bb, T) \quad (8)$$

The seed-level value-flow influence score is the cumulative value-flow influences of the basic blocks in its execution trace.

During fuzzing, we track the maximum ($\max VFS$) and minimum ($\min VFS$) value-flow influence scores of all seeds for final-score normalization. We define the normalized value-flow influence score $\tilde{VFS}(s, T)$ of seed s as follows:

$$\tilde{VFS}(s, T) = \frac{VFS(s, T) - \min VFS}{\max VFS - \min VFS} \quad (9)$$

C. Seed Scheduling

HF-DGF employs multi-dimensional feedback metrics, specifically control-flow distance, value-flow influence, and slice coverage, to direct seed prioritization and energy allocation in the fuzzing process. The following is a detailed explanation of this mechanism.

Seed Prioritization: Drawing on AFL [32], we implement a circular queue as the seed pool. New seeds are prioritized by their control-flow distances upon insertion, enabling HF-DGF to select seeds closer to the target earlier in the fuzzing process. To optimize performance, HF-DGF maintains pointers to every 100th seed in the queue, which streamlines queue maintenance and reduces runtime overhead.

Energy Allocation: DGF generally determines the mutation count for each seed based on its allocated energy. To generate more mutants from promising seeds, HF-DGF allocates more energy to seeds that are closer to the target, have higher value-flow influence scores, and exhibit greater slice coverage.

To address potential local optima, HF-DGF employs the simulated annealing algorithm independently on both control-flow distance and value-flow influence score. For control-flow distance, HF-DGF adapts AFLGo’s exponential cooling schedule T_{exp} . Concurrently, for the value-flow influence score, we introduce a novel annealing-based power schedule:

$$P_{\text{HF-DGF}}(s, T) = 2^{10 \cdot \tilde{VFS}(s, T) \cdot (1 - T_{\text{exp}}) + 0.5 T_{\text{exp}} - 5} \quad (10)$$

where $\tilde{VFS}(s, T)$ denotes the normalized value-flow influence score of seed s relative to target T , and T_{exp} is the shared cooling schedule from AFLGo’s distance-based annealing.

The final energy allocated to a certain seed is determined by integrating three dimensions: $P_{\text{AFL}}(s, T)$ (the energy assigned by AFL with slice coverage), $P_{\text{AFLGo}}(s, T)$ (the energy from AFLGo’s control-flow distance metric), and $P_{\text{HF-DGF}}(s, T)$ (the energy computed via HF-DGF’s value-flow influence score). The integrated energy $P(s, T)$ is calculated as the product of these components:

$$P(s, T) = P_{\text{AFL}}(s, T) \cdot P_{\text{AFLGo}}(s, T) \cdot P_{\text{HF-DGF}}(s, T) \quad (11)$$

This integration enables a comprehensive prioritization strategy that balances traditional coverage metrics, AFLGo’s control-flow distance, and novel value-flow analysis.

D. Selective Instrumentation

DGF enhances fuzzing by instrumenting the target program for runtime feedback, though instrumentation inevitably introduces runtime overhead—thus, balancing detailed feedback with overhead reduction is critical. HF-DGF adopts a non-one-size-fits-all strategy: we design three customized instrumentation approaches for distinct feedback dimensions. For coverage, we instrument only sliced basic blocks; for control-flow distance, we target boundary basic blocks; for value-flow influence, we instrument all blocks with value-flow scores. This strategy embodies a core philosophy: acquiring essential information at the lowest cost from code points with the highest information value, minimizing performance degradation while offering deep insights into program behavior across coverage, control-flow distance, and value-flow influence.

Instrumentation for Coverage Feedback: Traditional grey-box fuzzers indiscriminately gather coverage feedback from all basic blocks. In contrast, HF-DGF selectively acquires coverage feedback solely from the sliced basic blocks related to the targets. Specifically, HF-DGF first conducts slicing, using the target locations as the slicing criterion. Subsequently, it instruments only these sliced basic blocks to obtain coverage feedback. For a program P and a set of targets T , we define the slicing of T as follows:

$$\Psi(P, T) = SC(P, T) \vee SV(P, T) \quad (12)$$

where $SC(P, T)$ is the control-flow slicing and $SV(P, T)$ is the value-flow slicing.

Control-flow and value-flow slicing are both accomplished through a breadth-first backward traversal starting from the target location. Initially, HF-DGF performs function-level slicing on the target program using the function call graph and simultaneously extracts the call-site basic blocks invoking the sliced functions. Subsequently, for each sliced function, HF-DGF conducts control-flow slicing. It uses the call-site basic blocks in the control-flow graph as the slicing criterion. Regarding value-flow slicing, HF-DGF begins the operation on the value-flow graph, starting from the nodes where the target data is located.

Instrumentation for Distance Feedback: In HF-DGF, only boundary basic blocks are instrumented to provide distance feedback. Given a program P and all the sliced basic blocks $\Psi(P)$ of the target locations, the set of potential **Boundary Basic Blocks** of P , denoted as $\Omega(P)$, is defined as follows:

$$\Omega(P) = \{bb \in \Psi(P) \mid (Successors(bb) = NULL) \vee (\exists sbb \in Successors(bb) : sbb \notin \Psi(P))\} \quad (13)$$

where $Successors(bb)$ refers to the set of basic blocks that are the immediate successors of the basic block bb .

This definition embodies two crucial aspects. First, a boundary basic block must be among the sliced basic blocks. This ensures it contains target-relevant code and can provide valid distance feedback. Second, a boundary basic block either lacks successor nodes or has only non-sliced successor nodes, signifying its role as the final block in the execution path for distance feedback.

Leveraging boundary basic blocks, HF-DGF can acquire critical distance information, whether the program execution

is about to return to the sliced region or deviate from it. Instrumenting non-boundary basic blocks on target-reachable paths not only fails to yield extra valuable distance feedback but also imposes unnecessary runtime overhead. This insight aligns with the results of WindRanger ([23]) and Selectfuzz ([25]), both of which highlight that only deviation basic blocks are essential for analysis.

Instrumentation for Value-flow Influence Feedback : HF-DGF instruments all basic blocks with a value-flow influence score, driven by two key considerations. First, since the impact of each basic block along the execution path on the target data must be factored in, the value-flow influence score of a seed is computed by aggregating the scores of all relevant basic blocks on that path. Second, following HF-DGF’s thorough static analysis, only a limited number of basic blocks possess a value-flow influence score. Instrumenting these blocks will not cause a substantial decline in runtime performance.

V. IMPLEMENTATION

We developed a prototype of HF-DGF based on AFLGo [21], LLVM [33], and SVF [34]. Specifically, we constructed HF-DGF’s static analyzer with LLVM and SVF, writing approximately 1,300 lines of C++ code. This implementation encompasses hybrid slicing, control-flow distance calculation, value-flow influence score calculation, and the identification of boundary basic blocks. For hybrid feedback acquisition, we added 480 lines of C++ code to AFLGo’s LLVM pass for selective instrumentation. Additionally, we modified AFLGo’s scheduling algorithm by adding 460 lines and deleting 130 lines of C code. In total, HF-DGF consists of 10,832 lines of C and C++ code.

The source code for our prototype is available at <https://github.com/HF-DGF/HF-DGF>.

VI. EVALUATION

In this section, we assess the performance of HF-DGF using real-world vulnerabilities and seek answers to the following research questions:

- **RQ1:** How effective is HF-DGF at triggering known vulnerabilities?
- **RQ2:** How accurately can HF-DGF direct the fuzzing in terms of code coverage?
- **RQ3:** How efficient is the static analysis performed by HF-DGF?
- **RQ4:** How effective is the selective instrumentation strategy adopted by HF-DGF?
- **RQ5:** What impacts do each of the components have on the overall performance of HF-DGF?

A. Evaluation Setup

Baselines: We compare HF-DGF with the following four state-of-the-art fuzzers, which are publicly available:

- AFL [35]: v2.57b, Jul 5, 2020.
- AFLGo [21]: commit b170fad, May 8, 2022.
- WindRanger [23]: Docker hash 8614ceb.
- DAFL [22]: commit bdfed39, Dec 28, 2023.

- Beacon [36]: Docker hash a09c8cb.

We excluded Hawkeye [28] and Selectfuzz [25] from our comparison for the following reasons. Hawkeye is not publicly available. Regarding Selectfuzz, despite being partially open-source, we were unable to obtain and compile its static analyzer, which contains the core logic. We also attempt to evaluate the performance of AFL++ [37]. However, probably due to certain configuration-related factors, only the CVE-2017-5969 vulnerability was triggered, while other evaluation targets remained untriggered. Consequently, AFL++ is not included in Table II.

Benchmark: We evaluated fuzzers’ performance using various security vulnerabilities in C programs. Specifically, we adopted the 41 vulnerabilities from DAFL [22], detailed in Table I. As is common in vulnerability-exposing fuzzing efforts, we built all target binaries with ASAN (AddressSanitizer). But since Beacon doesn’t support fuzzing ASAN-compiled target binaries, we ran an extra experiment without ASAN to compare with Beacon.

Environment: The experiments were conducted on machines equipped with an AMD(R) EPYC 9354 CPU @ 3.80GHz, 256GB of memory, and running Ubuntu 20.04 LTS. Each fuzzing session took place within a Docker container [38], with 1 CPU core and 4GB of memory allocated. Of the 64 available CPU cores, only 54 were used, all within the same fuzzing session. For all fuzzers, the fuzzing phase was given a 24-hour time budget. To reduce the impact of fuzzing’s inherent randomness, the experiments were repeated 20 times, and the median value was computed.

B. Time-to-Exposure (RQ1)

We initiate the evaluation of HF-DGF’s effectiveness in terms of Time-To-Exposure (TTE) through the crash reproduction experiment. The results are presented in Table II. When a fuzzer fails to reproduce the target crash within 24 hours in over half of the 20 trials, making it impossible to obtain the median data, we mark the result as Not Available (N.A.).

After excluding the 9 cases where no fuzzing tool could obtain a median value, HF-DGF was able to report a median Time-To-Exposure (TTE) for 29 benchmarks. By comparison, AFL, AFLGo, WindRanger, and DAFL reported median TTEs for 25, 26, 20, and 28 benchmarks respectively. Additionally, among the remaining 32 cases, HF-DGF outperformed the other fuzzing tools in 18 instances. In contrast, AFL, AFLGo, WindRanger, and DAFL outperformed the rest in only 4, 2, 0, and 8 cases respectively. For the 20 benchmarks where all the tools successfully reported a median TTE, on average, HF-DGF was roughly 5.05 times faster than AFL, 5.79 times faster than AFLGo, a remarkable 73.75 times faster than WindRanger, and 2.56 times faster than DAFL. Furthermore, for the target vulnerabilities CVE-2018-7868, CVE-2018-11225, and CVE-2019-12982, where all other fuzzing tools faced challenges in reproducing the crashes, HF-DGF demonstrated a significant performance advantage over them.

In the supplementary experiment without AddressSanitizer, HF-DGF reported TTEs for 25 benchmarks. In comparison, DAFL and Beacon did so for only 16 and 20 benchmarks,

TABLE I: Vulnerability Information. The "Type" column indicates the vulnerability types using these abbreviations: **BOF** (Buffer Overflow), **ND** (Null Dereference), **SO** (Stack Overflow), **UAF** (Use-After-Free), **IO** (Integer Overflow), **OOM** (Out of Memory).

Project	Program	Version	CVE	Target	Type
LibMing	swftophp	0.4.7	2016-9827	outputscript.c:1687	BOF
			2016-9829	parser.c:1656	ND
			2016-9831	parser.c:66	BOF
			2017-9988	parser.c:2995	ND
			2017-11728	decompile.c:1699	ND
			2017-11729	decompile.c:1440	ND
			2017-7578	parser.c:68	BOF
	0.4.8	2018-7868	decompile.c:398	UAF	
		2018-8807	decompile.c:349	UAF	
		2018-8962	decompile.c:398	UAF	
		2018-11095	decompile.c:1843	UAF	
		2018-11225	decompile.c:2015	BOF	
		2018-11226	decompile.c:2015	BOF	
		2018-20427	decompile.c:425	ND	
		2019-9114	decompile.c:259	BOF	
		2019-12982	decompile.c:3120	BOF	
		2020-6628	decompile.c:2015	BOF	
		Lrzip	lrzip	0.631	2017-8846
2018-11496	stream.c:1756				UAF
cxxfilt	2.6	2016-4487	cplus-dem.c:4319	ND	
		2016-4489	cplus-dem.c:3007	UAF	
		2016-4490	cp-demangle.c:1596	IO	
		2016-4491	cp-demangle.c:5472	SO	
		2016-4492	cplus-dem.c:3606	IO	
		2016-6131	cplus-dem.c:4231	SO	
	objcopy	2.8	2017-8393	elf.c:3562	BOF
			2017-8394	objcopy.c:1482	ND
			2017-8395	cache.c:336	ND
	Bintuils	objdump	2.8	2017-8392	libbfd.c:548
2017-8396				libbfd.c:615	BOF
2017-8397				reloc.c:885	BOF
2017-8398				dwarf.c:484	BOF
2.31.1		2018-17360	libbfd.c:656	BOF	
strip	2.7	2017-7303	elf.c:1252	ND	
nm	2.9	2017-14940	elf.c:8205	OOM	
readelf	2.9	2017-16828	dwarf.c:7019	IO	
Libxml2	xmllint	2.9.4	2017-5969	valid.c:1181	ND
			2017-9047	valid.c:1279	BOF
			2017-9048	valid.c:1323	BOF
Libjpeg	cjpeg	1.5.90	2018-14498	rdbmp.c:209	BOF
		2.0.4	2020-13790	rdppm.c:434	BOF
# Total	10		41		6

respectively. Additionally, HF-DGF outperformed DAFL and Beacon in 21 cases, while DAFL and Beacon were superior in just 2 and 3 cases, respectively. In scenarios where all three tools provided median TTEs, HF-DGF was on average 20.87 times faster than DAFL and 8.45 times faster than Beacon.

We further investigated the fuzzers' affinity for different types of vulnerabilities. The results are shown in Table III. HF-DGF surpasses all others in reproducing four cases of use-after-free (UAF) vulnerabilities, while no other fuzzer can reproduce the remaining three UAF vulnerabilities. Only HF-DGF and DAFL successfully reproduce one of the two Stack Overflow vulnerabilities, and all the tested fuzzers fail to reproduce the other. Additionally, none of the evaluated fuzzers show the ability to reproduce the Out-of-Memory vulnerability. For various vulnerability types, HF-DGF exhibits an affinity comparable to that of other tools.

In summary, experimental results show that our proposed HF-DGF markedly boosts the performance of crash reproduction. Leveraging both distance and value-flow influence feedback, HF-DGF can comprehensively explore code segments distant from the target yet affecting its state space. This essentially strengthens HF-DGF's potential to unearth deeply hidden vulnerabilities.

C. Code Coverage (RQ2)

Subsequently, we evaluated HF-DGF's directional ability in fuzzing. From the 41 evaluation cases mentioned above, we chose the 18 top-performing targets according to the TTE HF-DGF achieved. Next, we acquired HF-DGF's coverage metrics and compared them with those of all baseline fuzzers. The representative average, based on 20 iterations, is shown in Fig. 4.

In all 18 test cases, HF-DGF exhibited the lowest code coverage, being 16.81 times lower than AFL, 18.45 times lower than AFLGo, 18.16 times lower than WindRanger, and 3.71 times lower than DAFL. Nevertheless, HF-DGF triggered the target vulnerabilities in all cases. This shows that even with a narrow exploration scope, HF-DGF did not overlook any of these vulnerabilities.

The proposed static analysis method significantly contributes to this success. By precisely computing control-flow distances and value-flow influence scores, HF-DGF effectively prioritizes fuzzing time towards reaching the target location and exploring the target state space. It focuses on parts closely linked to the target vulnerability and reduces the exploration of irrelevant code.

D. Performance of Static Analyzer (RQ3)

In directed grey-box fuzzing, the time for static analysis is usually not a one-off cost, especially in continuous fuzzing with frequent code modifications. Static analysis must be repeated after each modification. Thus, we evaluate both the time overhead of static analysis and the time proportion of each component in it.

Overhead of Static Analyzer: Figure 5 compares the static-analysis-phase times of AFLGo, Beacon, DAFL, and our proposed HF-DGF. Evidently, HF-DGF is far more efficient in static analysis, needing much less time than the others. On average, HF-DGF analyzes 44.56 times faster than AFLGo, 12.89 times faster than Beacon, and 2.75 times faster than DAFL. Its quicker static analysis allows the fuzzing phase to start earlier, which is crucial for urgent security testing.

TABLE II: Crash reproduction results of HF-DGF and the baseline tools. Each TTE represents the median value from 20 repeated experiments. **N.A.** indicates that the tool was unable to produce a median TTE, meaning it failed to reproduce the bug in more than half of the repeated experiments. The best result for each target (row) is highlighted in bold font. If no tool can successfully obtain the median TTE for a target, it is marked with bold font and an asterisk in the CVE column. **#TTE** denotes the number of successfully produced median TTEs by the tool. **#Best Perf.** denotes the number of best performances achieved by the tool among all fuzzers.

CVE	With ASAN									Without ASAN				
	AFL		AFLGo		WindRanger		DAFL		HF-DGF	DAFL		Beacon		HF-DGF
	TTE	Factor	TTE	Factor	TTE	Factor	TTE	Factor	TTE	TTE	Factor	TTE	Factor	TTE
2016-9827	88	3.52	68	2.72	59	2.36	52	2.08	25	130	1.29	2110	20.89	101
2016-9829	444	5.48	137	1.69	1865	23.02	101	1.25	81	1015	-	11335	-	N.A.
2016-9831	280	3.73	267	3.56	N.A.	-	137	1.83	75	335	3.10	223	2.06	108
2017-9988	157	0.23	3455	5.10	1275	1.88	1128	1.66	678	6480	8.47	2892	3.78	765
2017-11728	1360	10.97	2578	20.79	2001	16.14	202	1.63	124	N.A.	-	N.A.	-	537
2017-11729	518	9.42	413	7.51	714	12.98	56	1.02	55	280	2.57	3430	31.47	109
2017-7578	517	8.48	185	3.03	N.A.	-	37	0.61	61	1546	7.47	1366	6.60	207
2018-7868	N.A.	-	N.A.	-	N.A.	-	11746	2.19	5359	N.A.	-	N.A.	-	6273
2018-8807*	N.A.	-	N.A.	-	N.A.	-	N.A.	-	N.A.	N.A.	-	N.A.	-	N.A.
2018-8962*	N.A.	-	N.A.	-	N.A.	-	N.A.	-	N.A.	N.A.	-	N.A.	-	N.A.
2018-11095	2799	7.46	2523	6.73	837	2.23	537	1.43	375	2088	1.91	6065	5.54	1094
2018-11225	N.A.	-	16849	1.75	N.A.	-	N.A.	-	9626	N.A.	-	63641	17.19	3702
2018-11226	4313	0.61	N.A.	-	N.A.	-	5928	0.83	7128	N.A.	-	N.A.	-	5015
2018-20427	2761	1.49	4602	2.49	4946	2.67	9701	5.24	1851	29003	25.76	1574	1.40	1126
2019-9114	19310	-	7962	-	84885	-	N.A.	-	N.A.	N.A.	-	16681	2.28	7308
2019-12982	N.A.	-	13695	2.42	N.A.	-	N.A.	-	5668	N.A.	-	N.A.	-	N.A.
2020-6628	72988	4.02	31732	1.75	N.A.	-	41132	2.26	18167	25726	4.25	N.A.	-	6047
2017-8846*	N.A.	-	N.A.	-	N.A.	-	N.A.	-	N.A.	N.A.	-	N.A.	-	N.A.
2018-11496	17	5.67	26	8.67	9	3.00	8	2.67	3	2	1.00	N.A.	-	2
2016-4487	407	5.02	259	3.20	183	2.26	143	1.77	81	134	3.62	101	2.73	37
2016-4489	533	3.68	826	5.70	231	1.59	1137	7.84	145	1451	38.18	191	5.03	38
2016-4490	178	2.54	445	6.36	99	1.41	46	0.66	70	39	3.25	42	3.50	12
2016-4491	N.A.	-	N.A.	-	N.A.	-	N.A.	-	N.A.	N.A.	-	N.A.	-	11710
2016-4492	1909	1.12	3385	1.98	1003	0.59	891	0.52	1708	817	1.56	753	1.43	525
2016-6131	N.A.	-	N.A.	-	N.A.	-	N.A.	-	50063	N.A.	-	N.A.	-	N.A.
2017-8393	707	0.04	896	0.05	1280	0.07	1228	0.07	17601	N.A.	-	N.A.	-	N.A.
2017-8394	643	2.82	668	2.93	946	4.15	251	1.10	228	N.A.	-	1458	19.97	73
2017-8395	88	0.02	86	0.02	101	0.03	8	0.00	3879	N.A.	-	12	0.00	3944
2017-8392	298	0.09	341	0.10	N.A.	-	15	0.00	3270	N.A.	-	48339	1.08	44661
2017-8396*	N.A.	-	N.A.	-	N.A.	-	N.A.	-	N.A.	N.A.	-	N.A.	-	N.A.
2017-8397*	N.A.	-	N.A.	-	N.A.	-	N.A.	-	N.A.	N.A.	-	N.A.	-	N.A.
2017-8398	709	0.04	3551	0.22	1138	0.07	4359	0.27	16384	N.A.	-	N.A.	-	N.A.
2018-17360*	N.A.	-	N.A.	-	N.A.	-	N.A.	-	N.A.	N.A.	-	N.A.	-	N.A.
2017-7303	91	0.02	84	0.02	153	0.03	166	0.03	4934	221	0.26	14	0.02	840
2017-14940*	N.A.	-	N.A.	-	N.A.	-	N.A.	-	N.A.	N.A.	-	N.A.	-	N.A.
2017-16828	145	4.68	124	4.00	212	6.84	131	4.23	31	N.A.	-	N.A.	-	N.A.
2017-5969	198	33.00	192	32.00	1292	215.33	96	16.00	6	348	174.00	51	25.50	2
2017-9047	N.A.	-	N.A.	-	N.A.	-	16067	0.30	52814	N.A.	-	4340	0.16	27025
2017-9048	N.A.	-	N.A.	-	N.A.	-	5214	-	N.A.	N.A.	-	N.A.	-	N.A.
2018-14498	N.A.	-	N.A.	-	N.A.	-	7382	-	N.A.	N.A.	-	N.A.	-	N.A.
2020-13790*	N.A.	-	N.A.	-	N.A.	-	N.A.	-	N.A.	N.A.	-	N.A.	-	N.A.
# TTE (33/41)	25		26		20		28		29	16		20		25
# Best Perf.	4		2		0		8		18	2		3		21

Overhead of Each Component: We evaluated the time consumption of each component in HF-DGF’s static analysis phase, as shown in Fig. 6. Pointer analysis and constructing the

Sparse Value-Flow Graph (SVFG) took up most of the time, accounting for 45% and 35% respectively. These substantial time costs highlight potential areas for optimizing static anal-

TABLE III: Crash reproduction results grouped by type. Results are presented in the format **#Best/#TTE**, where **#TTE** represents the number of median TTE successfully produced by the tool, and **#Best** represents the number of best performances achieved by the tool among all the fuzzers.

Vulnerability Type	# Total	With ASAN					Without ASAN		
		AFL	AFLGo	WindRanger	DAFL	HF-DGF	DAFL	Beacon	HF-DGF
Buffer Overflow	17	3 / 8	1 / 9	0 / 4	4 / 10	5 / 10	0 / 4	1 / 6	7 / 8
Null Dereference	11	1 / 11	1 / 11	0 / 10	2 / 11	7 / 11	1 / 7	2 / 10	7 / 10
Use-After-Free	7	0 / 3	0 / 3	0 / 3	0 / 4	4 / 4	1 / 3	0 / 2	4 / 4
Integer Overflow	3	0 / 3	0 / 3	0 / 3	2 / 3	1 / 3	0 / 2	0 / 2	2 / 2
Stack Overflow	2	0 / 0	0 / 0	0 / 0	1 / 1	1 / 1	0 / 0	0 / 0	1 / 1
Out of Memory	1	0 / 0	0 / 0	0 / 0	0 / 0	0 / 0	0 / 0	0 / 0	0 / 0

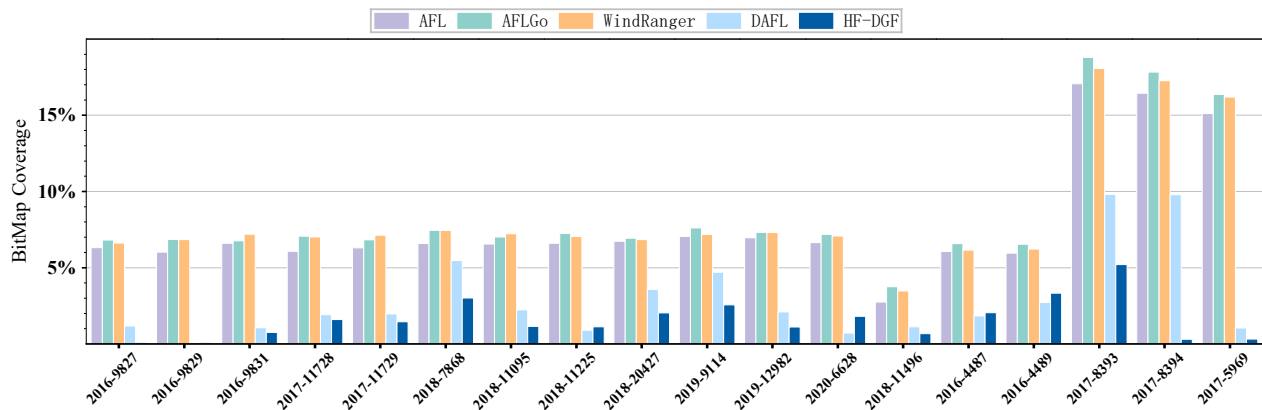


Fig. 4: BitMap Coverage

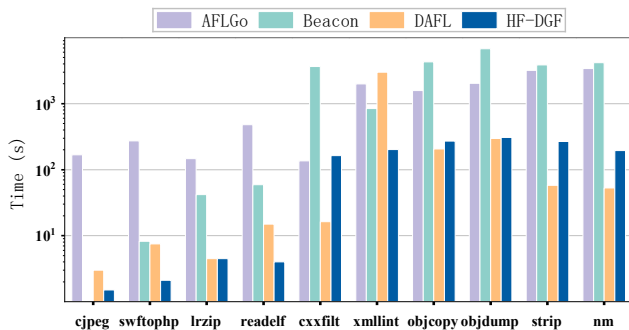


Fig. 5: Static Analyzer Time

ysis. By improving the algorithms for pointer analysis and SVFG construction, we anticipate further cutting down the static-analysis time and boosting the overall efficiency of the fuzzing process.

E. Effectiveness of Selective Instrumentation Strategy (RQ4)

We evaluated the effectiveness of HF-DGF’s selective instrumentation strategy on performance improvement, and the relevant statistical results are presented in Table IV.

For each target vulnerability, we quantified several key metrics: the total number of basic blocks in the target pro-

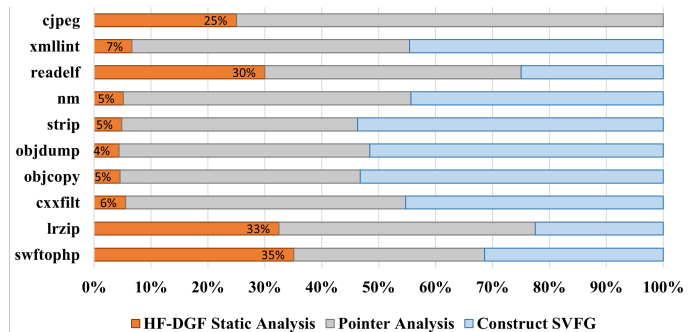


Fig. 6: Static Analysis Component Time Consumption

gram (**#BB**), the number of basic blocks instrumented for coverage feedback (**#Cov-Ins**), the number of target-reachable basic blocks (**#Dis-BB**), the number of boundary basic blocks instrumented for control-flow distance feedback (**#Dis-Ins**), and the number of basic blocks instrumented for value-flow feedback (**#Val-Ins**).

The results show that our selective instrumentation strategy substantially cuts down the number of basic blocks that need to be instrumented for coverage feedback (by 76.04%) and control-flow distance feedback (by 76.57%). Notably, even though all basic blocks with value-flow influence scores are instrumented, they merely make up 0.28% of the total basic

TABLE IV: Impact of Selective Instrumentation Strategy. **#BB** denotes the total quantity of basic blocks, **#Cov-Ins** represents the number of basic blocks instrumented for coverage feedback, **#Dis-BB** refers to the number of target-reachable basic blocks, **#Dis-Ins** is the number of boundary basic blocks instrumented for control-flow distance feedback, and **#Val-Ins** stands for the number of basic blocks instrumented to offer value-flow feedback.

Program	#BB	#Cov-Ins	#Dis-BB	#Dis-Ins	#Val-Ins
swftophp	3700	450	379	87	96
lrzip	9198	772	337	42	31
cxxfilt	42170	950	750	180	123
objcopy	51491	10633	10404	2397	350
objdump	58730	15979	15730	3648	126
strip	50788	15434	15212	3529	36
nm	45190	14786	14771	3326	18
readelf	18850	533	533	31	2
xmllint	69907	25683	25355	6317	192
cjpeg	5888	55	52	15	15
Ratio		23.96%		23.43%	0.28%

blocks.

Employing the selective instrumentation strategy, HF-DGF precisely hones its exploration in sliced basic code blocks closely linked to the target location. Although HF-DGF drastically cuts down the number of instrumented basic code blocks, it fully preserves the capacity to unearth target vulnerabilities, as validated in §VI-B.

F. Ablation Study (RQ5)

In this section, we examine the impact of the techniques employed on HF-DGF’s performance. To do so, we instantiated three variants of HF-DGF, as follows:

- **HF-DGF_noDist:** This variant omits backward-stepping distance calculation and adopts AFLGo’s distance-calculation approach.
- **HF-DGF_noSelect:** It lacks the selective instrumentation.
- **HF-DGF_noValue:** This one does not incorporate value-flow influence feedback.

We compared HF-DGF with its variants on 18 vulnerabilities. The TTE gaps between them and HF-DGF, as shown in Fig. 7, clarify the performance differences. Points above the axis of $y = 0$ (the solid red line) indicate that a variant takes longer to trigger crashes than HF-DGF; points below it mean a shorter time is taken.

Each technique independently provides positive guidance for HF-DGF, enhancing its performance. HF-DGF_noDist, HF-DGF_noSelect, and HF-DGF_noValue are 2.08, 3.86, and 7.46 times faster than AFLGo respectively. When combined, these techniques enable HF-DGF to consistently outpace AFLGo, reproducing vulnerabilities 6.98 times faster on average, demonstrating their synergistic effect.

VII. DISCUSSION

In this section, we discuss the limitations of HF-DGF and possible future work.

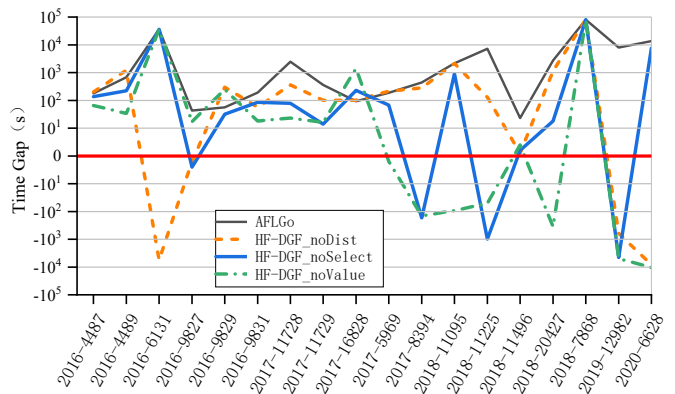


Fig. 7: Ablation of HF-DGF.

A. Solving Complex Constraints

HF-DGF employs random mutations to generate inputs for solving path constraints and data constraints, but it may not be sufficiently effective in solving complex constraints. Solving complex constraints, which involve reaching deep code locations and inducing specific values for variables, poses a common challenge in fuzzing. Recent studies have proposed various techniques such as symbolic executions [39], [40], taint tracking [41]–[44], and structure-aware mutations [7], [45] to enhance the capability of fuzzers in generating high-quality inputs. Other works trigger sequence-sensitive vulnerabilities by controlling the order of execution. For instance, DDRace [46] exploits concurrent UAF vulnerability by controlling thread interleaving while SCDF [47] and SDFuzz [48] generate inputs that can reach the target in order. Integrating HF-DGF with these techniques could enhance its ability to solve complex constraints.

B. The over-tainting issue in static analysis

Some programs, such as parsers and state machines, connect a large number of functions via dispatch functions. However, typically only one or a few functions are relevant to the target. Existing directed fuzzers often waste a considerable amount of time exploring new but irrelevant functions. HF-DGF try to reduce the misguidance caused by irrelevant functions through hybrid slicing. Though our adopted pointer analysis in slicing is structure-sensitive; however, the current implementation fails to differentiate between different regions of the input, and thus cannot associate functions that parse specific regions accurately. As a result, HF-DGF can still be misled by certain pointers, leading to the inclusion of target-unrelated functions in its exploration scope. For instance, during the evaluation of vulnerabilities like CVE-2017-8395, HF-DGF was found to underperform other baseline fuzzers that do not utilize pointer analysis.

In our future work, we intend to employ advanced static analysis techniques for dispatch function-related pointers, such as roughly determining the reference region through a symbolic execution engine [49]. This lightweight approach only requires distinguishing between regions without involving

complex solving, thereby avoiding substantial performance overhead.

VIII. RELATED WORK

In this section, we focus on discussing the most related works: control-flow guided directed fuzzing, data-flow guided directed fuzzing, and methods for reducing runtime overhead.

A. Control-flow Guided Directed Fuzzing

DGF enhances directionality by prioritizing and allocating more energy to seeds that are in closer proximity to the target, as measured using control-flow distance. AFLGo [21] initially introduced this distance metric and proposed a methodology for computing the distance between a seed trace and target sites. Accurate calculation of the distance is crucial to avoid any bias towards specific traces. Hawkeye [28] augments the adjacent-function distance by analyzing the frequency and distribution of function calls. WindRanger [23], instead of focusing on all basic blocks, calculates the distance through deviation blocks which act as critical basic blocks impeding inputs from reaching the target site, thereby enhancing DGF’s efficiency. In contrast to calculating distances during static analysis phase, Parmesan [50] computes distances based on dynamically constructed control-flow graphs. PDGF [51] obtains predecessors through ICFG static analysis and dynamically augments them with execution feedback.

B. Dataflow-Guided Directed Fuzzing

Data-sensitive vulnerabilities are only triggered under specific program states, not merely by reaching the target location. Consequently, existing work utilizes data flow to guide fuzzing in exploring program states. According to the stage at which data flow takes effect, existing works can be divided into the following two categories:

Static Data Flow Analysis. DDFuzz [52] and DataFlow [53] extend coverage feedback metrics by detecting new data-flow edge coverage. DAFL [22] analyzes data dependencies through the Def-Use Graph (DUG) and guides seed scheduling based on semantic relevance scores. CAFL [54] strengthens DGF by prioritizing crash targets using ordered vulnerability traces from crash dumps and patch analysis. Although its sequential constraint-solving mechanism boosts intentional crash exposure, it restricts path exploration with predefined solution sequences, limiting the discovery of novel vulnerabilities outside established paths.

Dynamic Data Flow Tracking. GreyOne [42] and WindRanger [23] use probing-based taint analysis to establish associations between input bytes and constraint variables. GreyOne then uses this mapping to decide which bytes to mutate, how to mutate them, and tune the fuzzing evolution direction. WindRanger adopts data-flow-sensitive mutation to better penetrate branch conditions. Nevertheless, runtime taint tracking introduces additional overhead and may not always yield desired outcomes.

HF-DGF integrates the benefits of static analysis and dynamic guidance by computing the value-flow influence of basic

blocks during static analysis and accumulating influence at runtime to direct fuzzing, thereby achieving a balance between speed and accuracy.

C. Methods for Reducing Runtime Overhead

Current research efforts focus on minimizing runtime overhead by terminating the program early and reducing instrumentation requirements.

Pruning-Guided Directed Fuzzing. Timely termination of the execution of unreachable inputs can reduce runtime overhead. Beacon [36] adopts lightweight static analysis to prune infeasible paths based on control-flow reachability and path-condition satisfiability. SieveFuzz [55] restricts execution within reachable regions by identifying unreachable boundaries and immediately terminating execution upon reaching the region boundaries.

Selective Instrumentation. DGF acquires feedback by instrumenting the target program, albeit at the cost of additional runtime overhead and a slowdown in the fuzzing process. Existing approaches mitigate this overhead through selective instrumentation. SelectFuzz [25] selectively instruments and explores only relevant code for fuzzing targets, including path-divergent and data-dependent code. DAFL [22] obtains coverage feedback solely from segments of the target program that are pertinent to the target location, identified through thin slicing performed on the DUG. DAFL exclusively performs instrumentation on all basic blocks within functions of the sliced DUG. While these selective instrumentation strategies reduce instrumentations, inaccurate analysis can result in insufficient feedback collection. To address this issue, our tool employs a multidimensional selective instrumentation strategy that precisely instruments necessary basic blocks without sacrificing feedback details.

IX. CONCLUSION

In this study, we present HF-DGF, a novel directed grey-box fuzzing framework leveraging hybrid runtime feedback, addressing three critical challenges with tailored solutions: our static analyzer uses a backward-stepping algorithm to compute basic block-level control-flow distances on a virtual ICFG for optimized seed prioritization; we introduce value-flow influence and define a value-flow influence score fitness metric to guide systematic exploration of target state spaces; and a selective instrumentation strategy mitigates runtime overhead from hybrid feedback by targeting critical code sections. Empirical evaluations on real-world vulnerabilities show that HF-DGF outperforms state-of-the-art fuzzers like AFL, AFLGo, WindRanger, DAFL, and Beacon in crash reproduction speed and code coverage efficiency.

REFERENCES

- [1] M. Böhme, V. J. Manès, and S. K. Cha, “Boosting fuzzer efficiency: An information theoretic perspective,” in *Proceedings of the 28th ACM Joint Meeting on European Software Engineering Conference and Symposium on the Foundations of Software Engineering*, 2020, pp. 678–689.
- [2] A. Fioraldi, D. C. D’Elia, and E. Coppa, “WEIZZ: Automatic grey-box fuzzing for structured binary formats,” in *Proceedings of the 29th ACM SIGSOFT international symposium on software testing and analysis*, 2020, pp. 1–13.

- [3] V. J. Manès, H. Han, C. Han, S. K. Cha, M. Egele, E. J. Schwartz, and M. Woo, "The art, science, and engineering of fuzzing: A survey," *IEEE Transactions on Software Engineering*, vol. 47, no. 11, pp. 2312–2331, 2019, publisher: IEEE.
- [4] B. Mathis, R. Gopinath, M. Mera, A. Kampmann, M. Hörschele, and A. Zeller, "Parser-directed fuzzing," in *Proceedings of the 40th acm sigplan conference on programming language design and implementation*, 2019, pp. 548–560.
- [5] B. Mathis, R. Gopinath, and A. Zeller, "Learning input tokens for effective fuzzing," in *Proceedings of the 29th ACM SIGSOFT international symposium on software testing and analysis*, 2020, pp. 27–37.
- [6] H. Han, D. Oh, and S. K. Cha, "CodeAlchemist: Semantics-aware code generation to find vulnerabilities in JavaScript engines," in *NDSS*, 2019.
- [7] J. Wang, B. Chen, L. Wei, and Y. Liu, "Superion: Grammar-aware greybox fuzzing," in *2019 IEEE/ACM 41st International Conference on Software Engineering (ICSE)*. IEEE, 2019, pp. 724–735.
- [8] J. Choi, K. Kim, D. Lee, and S. K. Cha, "NTFuzz: Enabling type-aware kernel fuzzing on windows with static binary analysis," in *2021 IEEE Symposium on Security and Privacy (SP)*. IEEE, 2021, pp. 677–693.
- [9] D. R. Jeong, K. Kim, B. Shivakumar, B. Lee, and I. Shin, "Razzer: Finding kernel race bugs through fuzzing," in *2019 IEEE Symposium on Security and Privacy (SP)*. IEEE, 2019, pp. 754–768.
- [10] S. Schumilo, C. Aschermann, R. Gawlik, S. Schinzel, and T. Holz, "{kAFL}::{Hardware-Assisted} feedback fuzzing for {OS} kernels," in *26th USENIX security symposium (USENIX Security 17)*, 2017, pp. 167–182.
- [11] X. Tan, Y. Zhang, J. Lu, X. Xiong, Z. Liu, and M. Yang, "SyzDirect: Directed Greybox Fuzzing for Linux Kernel," in *Proceedings of the 2023 ACM SIGSAC Conference on Computer and Communications Security*. Copenhagen Denmark: ACM, Nov. 2023, pp. 1630–1644. [Online]. Available: <https://dl.acm.org/doi/10.1145/3576915.3623146>
- [12] H. Gascon, C. Wressnegger, F. Yamaguchi, D. Arp, and K. Rieck, "Pulsar: Stateful black-box fuzzing of proprietary network protocols," in *Security and Privacy in Communication Networks: 11th EAI International Conference, SecureComm 2015, Dallas, TX, USA, October 26-29, 2015, Proceedings 11*. Springer, 2015, pp. 330–347.
- [13] D. Liu, V.-T. Pham, G. Ernst, T. Murray, and B. I. Rubinstein, "State selection algorithms and their impact on the performance of stateful network protocol fuzzing," in *2022 IEEE International Conference on Software Analysis, Evolution and Reengineering (SANER)*. IEEE, 2022, pp. 720–730.
- [14] J. Li, S. Li, G. Sun, T. Chen, and H. Yu, "Snpsfuzzer: A fast greybox fuzzer for stateful network protocols using snapshots," *IEEE Transactions on Information Forensics and Security*, vol. 17, pp. 2673–2687, 2022, publisher: IEEE.
- [15] X. Zhu and M. Böhme, "Regression Greybox Fuzzing," in *Proceedings of the 2021 ACM SIGSAC Conference on Computer and Communications Security*. Virtual Event Republic of Korea: ACM, Nov. 2021, pp. 2169–2182. [Online]. Available: <https://dl.acm.org/doi/10.1145/3460120.3484596>
- [16] P. Godefroid, M. Y. Levin, D. A. Molnar, and others, "Automated whitebox fuzz testing," in *NDSS*, vol. 8, 2008, pp. 151–166.
- [17] P. Godefroid, N. Klarlund, and K. Sen, "DART: Directed automated random testing," in *Proceedings of the 2005 ACM SIGPLAN conference on Programming language design and implementation*, 2005, pp. 213–223.
- [18] J. Xuan, X. Xie, and M. Monperrus, "Crash reproduction via test case mutation: Let existing test cases help," in *Proceedings of the 2015 10th joint meeting on foundations of software engineering*, 2015, pp. 910–913.
- [19] M. Soltani, A. Panichella, and A. Van Deursen, "Search-based crash reproduction and its impact on debugging," *IEEE Transactions on Software Engineering*, vol. 46, no. 12, pp. 1294–1317, 2018, publisher: IEEE.
- [20] W. Enck, P. Gilbert, S. Han, V. Tendulkar, B.-G. Chun, L. P. Cox, J. Jung, P. McDaniel, and A. N. Sheth, "Taintdroid: an information-flow tracking system for realtime privacy monitoring on smartphones," *ACM Transactions on Computer Systems (TOCS)*, vol. 32, no. 2, pp. 1–29, 2014, publisher: ACM New York, NY, USA.
- [21] M. Böhme, V.-T. Pham, M.-D. Nguyen, and A. Roychoudhury, "Directed greybox fuzzing," in *Proceedings of the 2017 ACM SIGSAC conference on computer and communications security*, 2017, pp. 2329–2344.
- [22] T. E. Kim, J. Choi, K. Heo, and S. K. Cha, "{DAFL}: Directed Greybox Fuzzing guided by Data Dependency," in *32nd USENIX Security Symposium (USENIX Security 23)*, 2023, pp. 4931–4948.
- [23] Z. Du, Y. Li, Y. Liu, and B. Mao, "WindRanger: a directed greybox fuzzer driven by deviation basic blocks," in *Proceedings of the 44th International Conference on Software Engineering*, 2022, pp. 2440–2451.
- [24] I. Haller, A. Slowinska, M. Neugschwandtner, and H. Bos, "Dowser: a guided fuzzer to find buffer overflow vulnerabilities," in *Proceedings of the 22nd USENIX Security Symposium*, 2013, pp. 49–64.
- [25] C. Luo, W. Meng, and P. Li, "Selectfuzz: Efficient directed fuzzing with selective path exploration," in *2023 IEEE Symposium on Security and Privacy (SP)*. IEEE, 2023, pp. 2693–2707.
- [26] L. O. Andersen, "Program analysis and specialization for the C programming language," 1994, publisher: Citeseer.
- [27] X. Li, X. Li, G. Lv, Y. Zhang, and F. Wang, "Directed Greybox Fuzzing with Stepwise Constraint Focusing," *arXiv preprint arXiv:2303.14895*, 2023.
- [28] H. Chen, Y. Xue, Y. Li, B. Chen, X. Xie, X. Wu, and Y. Liu, "Hawkeye: Towards a desired directed grey-box fuzzer," in *Proceedings of the 2018 ACM SIGSAC conference on computer and communications security*, 2018, pp. 2095–2108.
- [29] B. Steffen, J. Knoop, and O. Rüdthig, "The value flow graph: A program representation for optimal program transformations," in *ESOP'90: 3rd European Symposium on Programming Copenhagen, Denmark, May 15-18, 1990 Proceedings 3*. Springer, 1990, pp. 389–405.
- [30] S. Cherm, L. Princehouse, and R. Rugina, "Practical memory leak detection using guarded value-flow analysis," in *Proceedings of the 28th ACM SIGPLAN Conference on Programming Language Design and Implementation*, 2007, pp. 480–491.
- [31] Y. Sui and J. Xue, "SVF: interprocedural static value-flow analysis in LLVM," in *Proceedings of the 25th international conference on compiler construction*, 2016, pp. 265–266.
- [32] M. Zalewski, "American fuzzy lop," 2017.
- [33] C. Lattner and V. Adve, "LLVM: A compilation framework for lifelong program analysis & transformation," in *International symposium on code generation and optimization, 2004. CGO 2004*. IEEE, 2004, pp. 75–86.
- [34] Y. Sui and J. Xue, "Svf: interprocedural static value-flow analysis in llvm," in *Proceedings of the 25th international conference on compiler construction*, 2016, pp. 265–266.
- [35] M. Zalewski, "American fuzzy lop." [Online]. Available: <https://lcamtuf.coredump.cx/afl/>
- [36] H. Huang, Y. Guo, Q. Shi, P. Yao, R. Wu, and C. Zhang, "Beacon: Directed grey-box fuzzing with provable path pruning," in *2022 IEEE Symposium on Security and Privacy (SP)*. IEEE, 2022, pp. 36–50.
- [37] A. Fioraldi, D. Maier, H. Eißfeldt, and M. Heuse, "AFL++: Combining incremental steps of fuzzing research," in *14th USENIX Workshop on Offensive Technologies (WOOT 20)*. USENIX Association, Aug. 2020. [Online]. Available: <https://www.usenix.org/conference/woot20/presentation/fioraldi>
- [38] Docker, "What is a Container? | Docker." [Online]. Available: <https://www.docker.com/resources/what-container/>
- [39] N. Stephens, J. Grosen, C. Salls, A. Dutcher, R. Wang, J. Corbetta, Y. Shoshitaishvili, C. Kruegel, and G. Vigna, "Driller: Augmenting fuzzing through selective symbolic execution," in *NDSS*, vol. 16, 2016, pp. 1–16, issue: 2016.
- [40] I. Yun, S. Lee, M. Xu, Y. Jang, and T. Kim, "{QSYM}: A practical concolic execution engine tailored for hybrid fuzzing," in *27th USENIX Security Symposium (USENIX Security 18)*, 2018, pp. 745–761.
- [41] P. Chen and H. Chen, "Angora: Efficient fuzzing by principled search," in *2018 IEEE Symposium on Security and Privacy (SP)*. IEEE, 2018, pp. 711–725.
- [42] S. Gan, C. Zhang, P. Chen, B. Zhao, X. Qin, D. Wu, and Z. Chen, "{GREYONE}: Data flow sensitive fuzzing," in *29th USENIX security symposium (USENIX Security 20)*, 2020, pp. 2577–2594.
- [43] J. Liang, M. Wang, C. Zhou, Z. Wu, Y. Jiang, J. Liu, Z. Liu, and J. Sun, "Pata: Fuzzing with path aware taint analysis," in *2022 IEEE Symposium on Security and Privacy (SP)*. IEEE, 2022, pp. 1–17.
- [44] S. Chen, Z. Lin, and Y. Zhang, "{SelectiveTaint}: Efficient Data Flow Tracking With Static Binary Rewriting," in *30th USENIX Security Symposium (USENIX Security 21)*, 2021, pp. 1665–1682.
- [45] S. Cao, B. He, X. Sun, Y. Ouyang, C. Zhang, X. Wu, T. Su, L. Bo, B. Li, C. Ma, and others, "Oddfuzz: Discovering java deserialization vulnerabilities via structure-aware directed greybox fuzzing," in *2023 IEEE Symposium on Security and Privacy (SP)*. IEEE, 2023, pp. 2726–2743.
- [46] M. Yuan, B. Zhao, P. Li, J. Liang, X. Han, X. Luo, and C. Zhang, "DDRace: finding concurrency UAF vulnerabilities in Linux drivers with directed fuzzing," in *32nd USENIX Security Symposium, USENIX Security 2023, Anaheim, CA, USA, August 9-11, 2023*. [Online]. Available: <https://www.usenix.org/system/files/usenixsecurity23-yuan-ming.pdf>

- [47] H. Liang, L. Jiang, L. Ai, and J. Wei, "Sequence directed hybrid fuzzing," in *2020 IEEE 27th International Conference on Software Analysis, Evolution and Reengineering (SANER)*. IEEE, 2020, pp. 127–137.
- [48] P. Li, W. Meng, and C. Zhang, "SDFUZZ: Target States Driven Directed Fuzzing."
- [49] C. Cadar, D. Dunbar, D. R. Engler, and others, "Klee: Unassisted and automatic generation of high-coverage tests for complex systems programs." in *OSDI*, vol. 8, 2008, pp. 209–224.
- [50] S. Österlund, K. Razavi, H. Bos, and C. Giuffrida, "{ParmeSan}: Sanitizer-guided greybox fuzzing," in *29th USENIX Security Symposium (USENIX Security 20)*, 2020, pp. 2289–2306.
- [51] Y. Zhang, Y. Liu, J. Xu, and Y. Wang, "Predecessor-aware Directed Greybox Fuzzing." IEEE Computer Society, Oct. 2023, pp. 40–40, iSSN: 2375-1207. [Online]. Available: <https://www.computer.org/csdl/proceedings-article/sp/2024/313000a040/1RjEaeMELbq>
- [52] A. Mantovani, A. Fioraldi, and D. Balzarotti, "Fuzzing with data dependency information," in *2022 IEEE 7th European Symposium on Security and Privacy (EuroS&P)*. IEEE, 2022, pp. 286–302.
- [53] A. Herrera, M. Payer, and A. L. Hosking, "DatAFLow: Toward a data-flow-guided fuzzer," *ACM Transactions on Software Engineering and Methodology*, vol. 32, no. 5, pp. 1–31, 2023, publisher: ACM New York, NY, USA.
- [54] G. Lee, W. Shim, and B. Lee, "Constraint-guided directed greybox fuzzing," in *30th USENIX Security Symposium (USENIX Security 21)*, 2021, pp. 3559–3576.
- [55] P. Srivastava, S. Nagy, M. Hicks, A. Bianchi, and M. Payer, "One fuzz doesn't fit all: Optimizing directed fuzzing via target-tailored program state restriction," in *Proceedings of the 38th Annual Computer Security Applications Conference*, 2022, pp. 388–399.